



Upper Albian OAE 1d event in the Chihuahua Trough, New Mexico, U.S.A.



R.W. Scott ^{a,*}, Michael Formolo ^a, Natalie Rush ^a, Jeremy D. Owens ^b, Francisca Oboh-Ikuenobe ^c

^a Geosciences Department, University of Tulsa, 800 S. Tucker Dr., Tulsa, OK 74104, USA

^b Department of Earth Sciences, University of California, Riverside, CA 92521, USA

^c Department of Geological Sciences and Engineering, Missouri University of Science and Technology, Rolla, MO 65409-0410, USA

ARTICLE INFO

Article history:

Received 22 April 2013

Accepted in revised form 23 August 2013

Available online

Keywords:

Upper Albian

OAE 1d

Graphic correlation

Carbon isotopes

Sequential iron

Chihuahua Trough

ABSTRACT

Oceanic anoxic events are clues to ocean processes and are correlation datums. In North America only OAE 1a and 2 are well documented. Based on a low-resolution sampling program, a multi-proxy geochemical approach constrained by a biostratigraphic framework was utilized to identify OAE 1d in the upper part of the upper Albian Mesilla Valley Formation near El Paso, Texas. Chronostratigraphic and biostratigraphic evidence indicate that the OAE 1d event in the Mesilla Valley section is located in the lower part of the upper Albian–Cenomanian *Ovoidinium verrucosum* zone, which correlates with the uppermost Albian *Parathalassinella appenninica* and *Stoliczkaia dispar* zones. The chronostratigraphic age of the geochemical event in the Mesilla Valley Formation is uppermost Albian (97.39–97.30 Ma).

The classic geochemical signatures for OAEs are enriched total organic carbon (TOC) concentrations and coupled positive $\delta^{13}\text{C}$ excursions. OAE 1d at this location records TOC values ranging from 0.25 to 0.69 wt.% throughout the Mesilla Valley Formation, where TOC increases during the OAE (21.0–40.0 m) to more than 0.40 wt.%. Interestingly, the organic matter in the Mesilla Valley is dominantly type III, which indicates a pervasive terrigenous source. Although marine organic matter is abundant from the base into the middle of the proposed OAE interval, it is progressively replaced by terrestrial material above the OAE section during progradation. The $\delta^{13}\text{C}_{\text{Organic}}$ values record a positive $\delta^{13}\text{C}$ shift of +1.6‰ from –26.41 to –24.80‰ across the stratigraphic interval from 21.0 to 40.0 m, which correlates with OAE 1d.

Mn and Fe geochemistry suggest the depositional conditions of the Mesilla Valley Formation were dominated by anoxic and possibly Fe-rich bottom waters, specifically during the time period associated with the OAE 1d event. This interpretation is supported by the presence of Fe enrichment recorded by $\text{Fe}_{\text{Total}}/\text{Al}$ and $\text{Fe}_{\text{Highly Reactive}}/\text{Fe}_{\text{T}}$ with the lack of $\text{Fe}_{\text{Pyrite}}/\text{Fe}_{\text{Highly Reactive}}$ associated with Mn depletion.

© 2013 Elsevier Ltd. All rights reserved.

1. Introduction

During Cretaceous oceanic anoxic events (OAEs) widespread black, organic-rich shale was deposited in deep oceans and marginal basins. These strata represent short-term changes in marine productivity, burial and preservation of organic matter (Broecker and Peng, 1982). Six major Cretaceous events were discovered in deep-sea drilling records: early Aptian OAE 1a, Albian OAE 1b, 1c and 1d, Cenomanian–Turonian OAE 2, and Santonian OAE 3 (Schlanger and Jenkyns, 1976; Arthur et al., 1985, 1990; Jenkyns

and Wilson, 1999; Leckie et al., 2002). Deposition of these organic-rich beds was initially proposed to be related to high sea level and anaerobic ocean conditions (Arthur et al., 1985). The flooding of marginal shelf and exposed continental shelves stimulated primary production (Arthur et al., 1990; Erbacher et al., 1996). Erba (1994) and Jenkyns (2010) suggested that a change in oceanic productivity from calcareous planktic foraminifera and nannoplankton to organic-walled dinoflagellates and siliceous radiolaria was related to oceanic anoxic events when near-surface ocean nutrients increased. Hallam (1985) and Price (1999) also recognized the oscillation between arid and humid climates during the Cretaceous. During the humid periods enhanced weathering delivered increased clastic material and nutrients to the coastal regions while also promoting density stratification

* Corresponding author. Tel.: +1 918 243 5418.

E-mail address: rwscott@cimtel.net (R.W. Scott).

between the freshwater run-off and underlying marine water. These periods were also characterized by enhanced oceanic circulation further expanding upwelling and promoting primary production (Föllmi, 2012). In addition to oxygen depletion and stratification, the arid periods are characterized by reduced weathering and nutrient delivery (Föllmi, 2012). External mechanisms may have also promoted the establishment of OAEs. These include the formation of large igneous provinces (Arthur et al., 1990; Larson and Erba, 1999; Tejada et al., 2009), and clathrate destabilization and other methane sources, such as peatlands (Jahren et al., 2001; Emeis and Weissert, 2009). Föllmi (2012) provides an extensive review of these mechanisms. It is apparent that the presence of OAEs indicates the combination of many processes as a trigger. Recognizing these processes in the geologic record provides important information regarding the feedbacks, initiation, maintenance and termination of OAEs.

Isotope stratigraphy traditionally has been one of the proxies utilized to recognize and correlate OAEs. Conventionally, OAEs have been identified by a positive $\delta^{13}\text{C}$ shift of 1.5‰ or greater in organic and inorganic carbon (Jenkyns, 2010; Herrle et al., 2004). Carbon isotopic shifts have also been used as chronostratigraphic tools (Scholle and Arthur, 1980). However, certain OAEs (e.g., 1c; Erbacher et al., 1999), do not exhibit such diagnostic $\delta^{13}\text{C}$ excursions. Coupling isotope excursions with inorganic geochemical proxies aid in the reconstruction of depositional conditions and highlight the occurrence of OAE events when traditional signals may not be as apparent. Analyses of iron mineral speciation (e.g., Lyons and Severmann, 2006; Gill et al., 2011) and shifts in trace metal concentrations (e.g., Cruse and Lyons, 2004; Tribouillard et al., 2006; Gill et al., 2011) have been used to reconstruct paleoredox conditions during other periods of black shale deposition in Earth's history. When integrated in the proper biostratigraphic and isotopic context, the trace metal and sequential iron signatures can constrain the presence of an OAE that may not be apparent by utilizing more traditional approaches.

Recognition of Cretaceous OAE records in the Gulf Coast region of North America has been limited. At Peregrina Canyon, Tamaulipas, Mexico, both $\delta^{13}\text{C}$ and total organic carbon curves span from the Jurassic/Cretaceous boundary to the Campanian (Scholle and Arthur, 1980) and record OAE 1a and 1b (Bralower et al., 1999). In the North Texas outcrop section a thin $\delta^{13}\text{C}$ negative shift of nearly 1.5‰ at the top of the Pawpaw Formation was correlated with the Breistroffer interval in France (Reichelt, 2005). Near the Aptian–Albian Comanchean shelf margin in the South Texas subsurface OAEs 1a, 1b, and possibly 1d and 2 are identified in cores by carbon isotopes (Phelps, 2011), although in some cores biostratigraphic data is non-diagnostic. Phelps (2011) related these carbon isotope shifts to maximum flooding of shelf sequences and repeated drowning of the platform. In certain locations outside of the Gulf Coast, events such as the late Albian OAE 1c and in black shales from the Aptian–Albian boundary, strong $\delta^{13}\text{C}$ excursions in both inorganic and organic carbon are absent and the organic matter is dominantly terrestrial (Pratt and King, 1986; Erbacher et al., 1996). Similar geochemical signatures may be present throughout the Gulf Coast region, making it easy to overlook the presence of an OAE if $\delta^{13}\text{C}$ records are the primary line of evidence. The absence of the traditional isotope excursion requires additional geochemical evidence to constrain the presence of OAE 1d in the Gulf Coast region of the United States.

The objective of this study is to provide a stratigraphic framework and evidence of an OAE in the upper Albian Mesilla Valley Formation at Cerro de Cristo Rey, in Doña Ana County, southeastern-most New Mexico (Fig. 1). Based on a low resolution sampling program, an integrated geochemical approach, including $\delta^{13}\text{C}$ and $\delta^{18}\text{O}$, total organic and inorganic carbon concentrations,

iron mineral speciation, and manganese concentrations, were measured to constrain the depositional environment. These data are integrated with chronostratigraphic data to correlate the Mesilla Valley with standard upper Albian zonal schemes. Combined, these data constrain the presence of OAE 1d in the Mesilla Valley Formation in the Gulf Coast region.

2. Geologic setting

During the Cretaceous Period, global sea level fluctuated with an overall long-term rise that peaked in the Late Cretaceous (Skelton et al., 2003). By late Albian the Western Interior of North America was covered by an inland sea that periodically connected the Comanche Shelf in the subtropical Caribbean Province with the Boreal Province of the Arctic Ocean in the north. The Comanche Shelf formed the southern margin of North America during the Cretaceous; on its southwestern border in northern Chihuahua, Mexico, the Chihuahua Trough trends northwest–southeast (Scott, 2003; Fig. 2).

Cerro de Cristo Rey is on the northeastern shoulder of the Chihuahua Trough and at the entrance to the western side of the Western Interior Sea is (Fig. 2). It is an andesitic laccolith emplaced during the Eocene Epoch (Strain, 1968; Lovejoy, 1976) (Fig. 1). Late Albian to early Cenomanian strata are exposed on the northeast flank of Cerro de Cristo Rey. Upper Albian strata are up to 230 m thick. Sediment deposition occurred on an open shelf below or near wave base during periods of variable siliciclastic influx (Lucas et al., 2010). These strata grade south–southeast into upper Albian shale and calcarenite of the Benevides Formation and nodular limestone of the Loma Plata Formation in the Chihuahua Trough, which together are up to 260 m thick (Monreal and Longoria, 1999). The Mesilla Valley Formation is the candidate for an oceanic anoxic event because it comprises dark gray shale (suggestive of organic carbon enrichment) in the uppermost part of the upper Albian section at Cerro de Cristo Rey. It is overlain by the Mojado Formation, which in turn is overlain by basal lower Cenomanian Del Rio Formation.

Samples for whole-rock geochemical analysis were collected from two Mesilla Valley Formation outcrops along the NE flank of Cerro de Cristo Rey [N 31° 47.432, W 106° 32.162 (Kmv1) and N 31° 47.911, W 106° 32.318 (Kmv2)] (Fig. 1) (Rush, 2012). Samples from locations 1 and 2 are identified with the prefixes Kmv 1 and Kmv 2, respectively.

3. Stratigraphy of Cerro de Cristo Rey section

3.1. Lithostratigraphy

Cretaceous stratigraphic units exposed at Cerro de Cristo Rey were described by Böse (1910), formalized by Strain (1976) and Lovejoy (1976) and reviewed by Lucas et al. (2010) (Fig. 3). The Mesilla Valley Formation is a gray to grayish black, slope-forming shale containing thin (1–15 cm) sandstone lenses, oyster beds, and siderite beds. It is named for Mesilla Valley north of Cerro de Cristo Rey. A range of thicknesses has been reported for the formation at Cerro de Cristo Rey. This study measured a total thickness of 51 m, however Lucas et al. (2010) reported 65 m, Strain (1976) reported 64 m, Norland (1986) reported 60 m, and Lovejoy (1976) and Belle (1987) reported 55 m. Lovejoy (1976) recognized that the Mesilla Valley is faulted in some locations, which may account for the reported thickness variations. Lovejoy (1976) did not identify faults at the locations sampled for this study.

The Mesilla Valley Formation conformably overlies the uppermost limestone bed of the Muleros Formation and grades up into

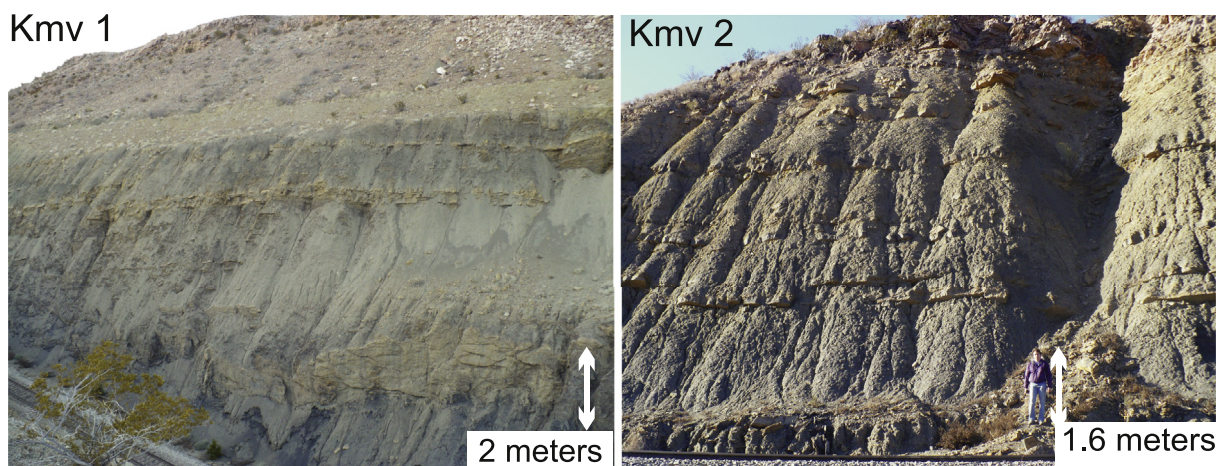
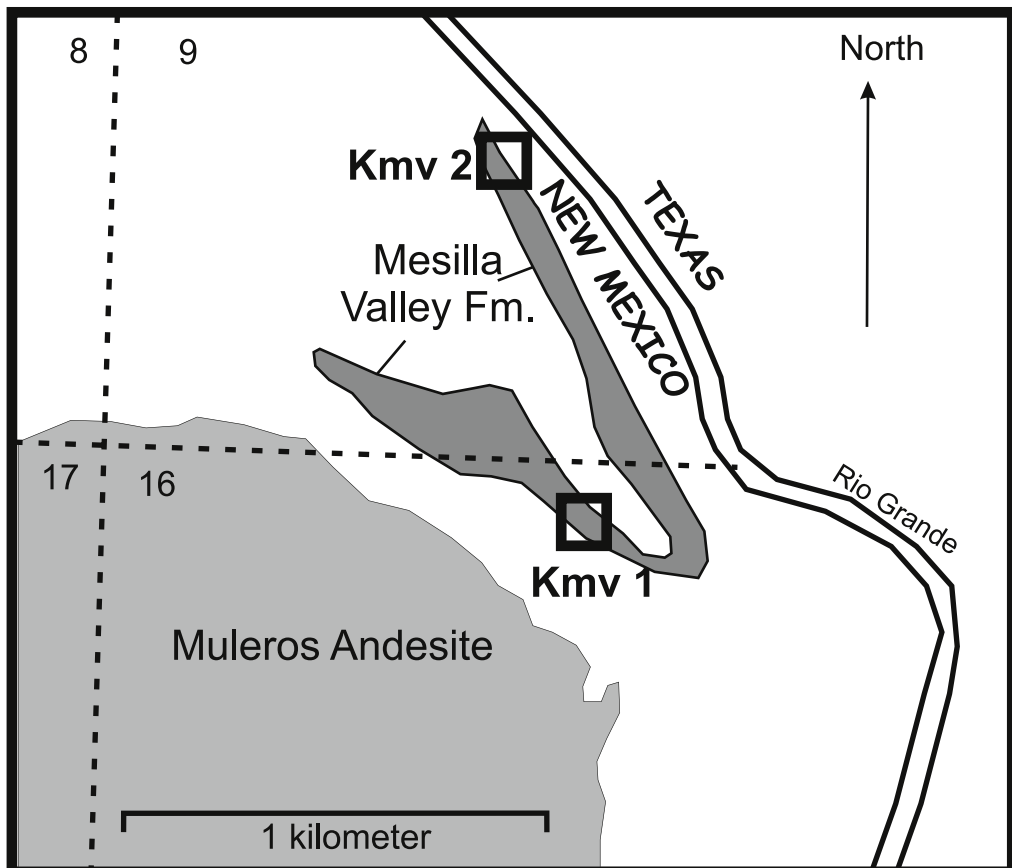


Fig. 1. Location of measured sections and outcrop samples of the Mesilla Valley Formation. Geologic map is from Lucas et al. (2010). Outcrop areas of sample locations KmV 1 (south) and KmV 2 (north) are outlined.

the Mojado Formation (synonym of Anapra Formation) by the addition of sandstone beds (Fig. 3). Lucas et al. (2010) reviewed the lithostratigraphy and sedimentary petrography of the Cretaceous strata at Cerro de Cristo Rey and proposed six unconformity-bounded depositional cycles that correlate with upper Albian depositional cycles in the North Texas reference section (Scott et al., 2001, 2003). The Mesilla Valley was correlated with the Weno and Pawpaw formations in north-central Texas. However, new palynostratigraphic data suggests that the Mesilla Valley correlates mainly with the Pawpaw Formation.

3.2. Biostratigraphy

The Order Ammonoidea is the principal fossil group that subdivides the Albian into zones and subzones (Reboulet et al., 2011). Important complementary fossil groups calibrated to Albian Tethyan ammonite zones are nannofossils (Bown et al., 1998), planktic and benthic foraminifera (Arnaud-Vanneau and Bilotte, 1998; Leckie et al., 2002), and dinoflagellates (Foucher and Monteil, 1998). Gulf Coast Lower Cretaceous ammonite biostratigraphy is correlated with the standard zones by both cosmopolitan

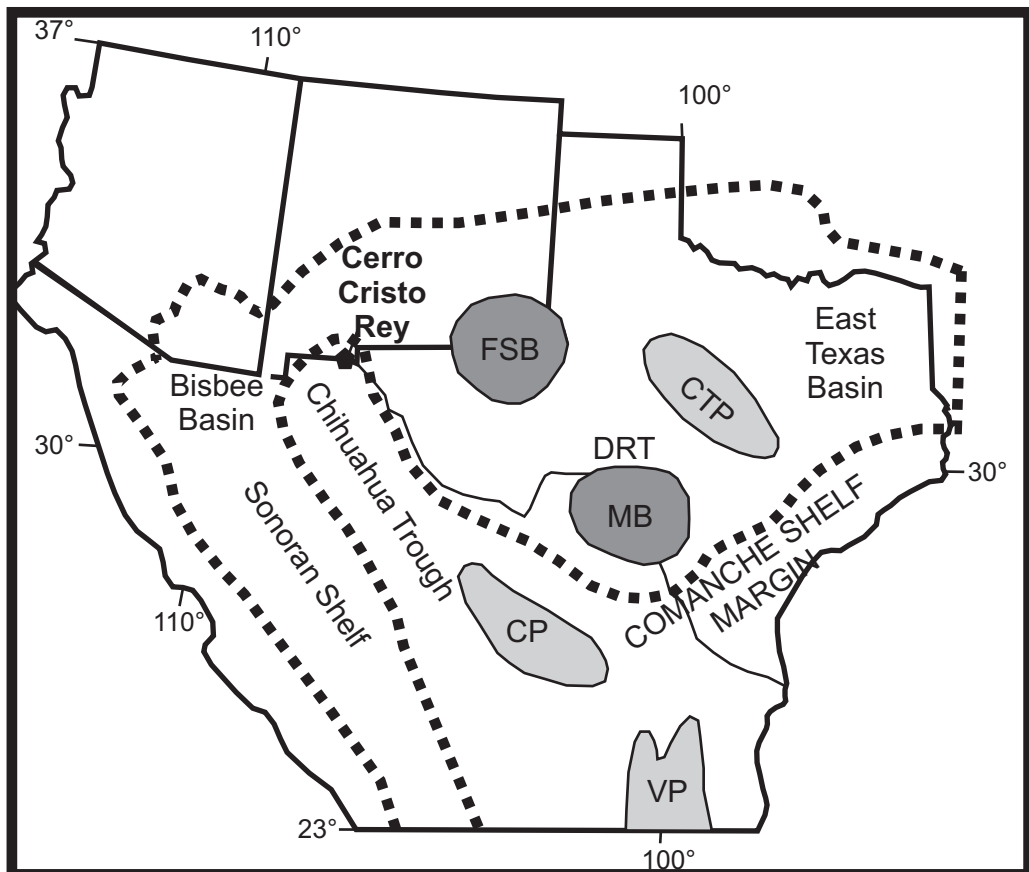


Fig. 2. Late Albian paleogeography of the Chihuahua Trough and the Cerro de Cristo Rey region (Scott, 2003). CP – Coahuila Platform, CTP – Central Texas Platform, FSB – Fort Stockton Basin, MB – Maverick Basin, VP – Valles Platform.

and endemic species that are documented in the North Texas reference section of the Fredericksburg and Washita Groups (Fig. 3) (Young, 1986; Kennedy et al., 1999, 2005; Scott et al., 2003). In the Cristo Rey section molluscan biostratigraphy is based on ammonoids and bivalves (Böse, 1910; Strain, 1976; Young, 1986; Lucas et al., 2010). However few of these zones correlate with the standard zones because of facies exclusion (Lucas et al., 2010). A detailed local biostratigraphy of the Cristo Rey section includes ammonites, bivalves, foraminifera, and dinoflagellate cysts (see online in *Supplementary Information*), and new palynological analyses of this study focused on the Mesilla Valley Formation.

The Mesilla Valley Formation is indirectly correlated with the European *Mortoniceras rostratum* and *Stoliczkaia dispar* zones by oysters and dinoflagellate cysts, which occur with Gulf Coast ammonites in the North Texas section (Fig. 3) (Young, 1986; Scott et al., 2003). Thin sandstone beds of the Mesilla Valley Formation yield the oyster, *Peiliinia quadruplicata* (Shumard) and the benthic foraminifer, *Cribratina texana* (Conrad). In the underlying Mulerios Formation the uppermost Albian *Texigryphaea washitaensis* (Hill) is abundant, and in the overlying Del Rio formation basal Cenomanian oysters are *Ilmatogyra arietina* (Roemer) and *Gyrostrea whitneyi* (Böse). These guide fossils indirectly correlate the Mesilla Valley with the Pawpaw Formation in North Texas and the *Mortoniceras wintoni* (Adkins) and the *Drakeoceras drakei* Young ammonoid zones. These zones correlate biostratigraphically with the upper Albian *Mortoniceras rostratum* Subzone of the *Stoliczkaia dispar* Zone in Europe (Fig. 3; Scott et al., 2003; Kennedy et al., 2005; Lucas et al., 2010).

This correlation is supported by the discovery of the dinoflagellate cyst, *Ovoidinium verrucosum* (Cookson and Hughes), in the

Mesilla Valley Formation; this distinctive microfossil is reported in the *S. dispar* Zone (Foucher and Monteil, 1998). Although the Mojado Formation has not yielded age-diagnostic fossils, it is overlain by the lower Cenomanian Del Rio Formation and the *Graysonites adkinsi* Zone, which correlates with the basal Cenomanian *Mantelliceras mantelli* Zone (Young, 1986; Kennedy et al., 2005).

3.3. Depositional environment and sequence stratigraphy

The Mesilla Valley Formation was deposited on a nearshore, muddy marine shelf below wave base (Lucas et al., 2010). Deposition shoaled up section from relatively deeper water represented by shale beds with rare thin sandstone lenses to shallower water with interbedded ripple-laminated sandstones and ferruginous sandstone beds (Strain, 1976; Lucas et al., 2010). The thin sandstone and oyster beds are interpreted as storm deposits (Lucas et al., 2010) similar to upper Albian density current sands of the Washita Group in North Texas (Scott et al., 1975).

The Lower Cretaceous units of the Cerro de Cristo Rey section correlate with depositional cycles defined in the North Texas section (Fig. 3) (Scott et al., 2003; Lucas et al., 2010). The six transgressive shoaling-up intervals are separated by sharp contacts between shallower- and deeper-water marine facies. The Mesilla Valley Formation and the lower part of the Mojado Formation together represent one deepening-shallowing depositional cycle and correlate with Al Wa 5 cycle defined by the middle and upper shale-limestone succession of the Pawpaw Formation (Scott et al., 2001, 2003; Lucas et al., 2010). The transgressive basal contact of the Mesilla Valley with the underlying Mulerios Formation is Al TS

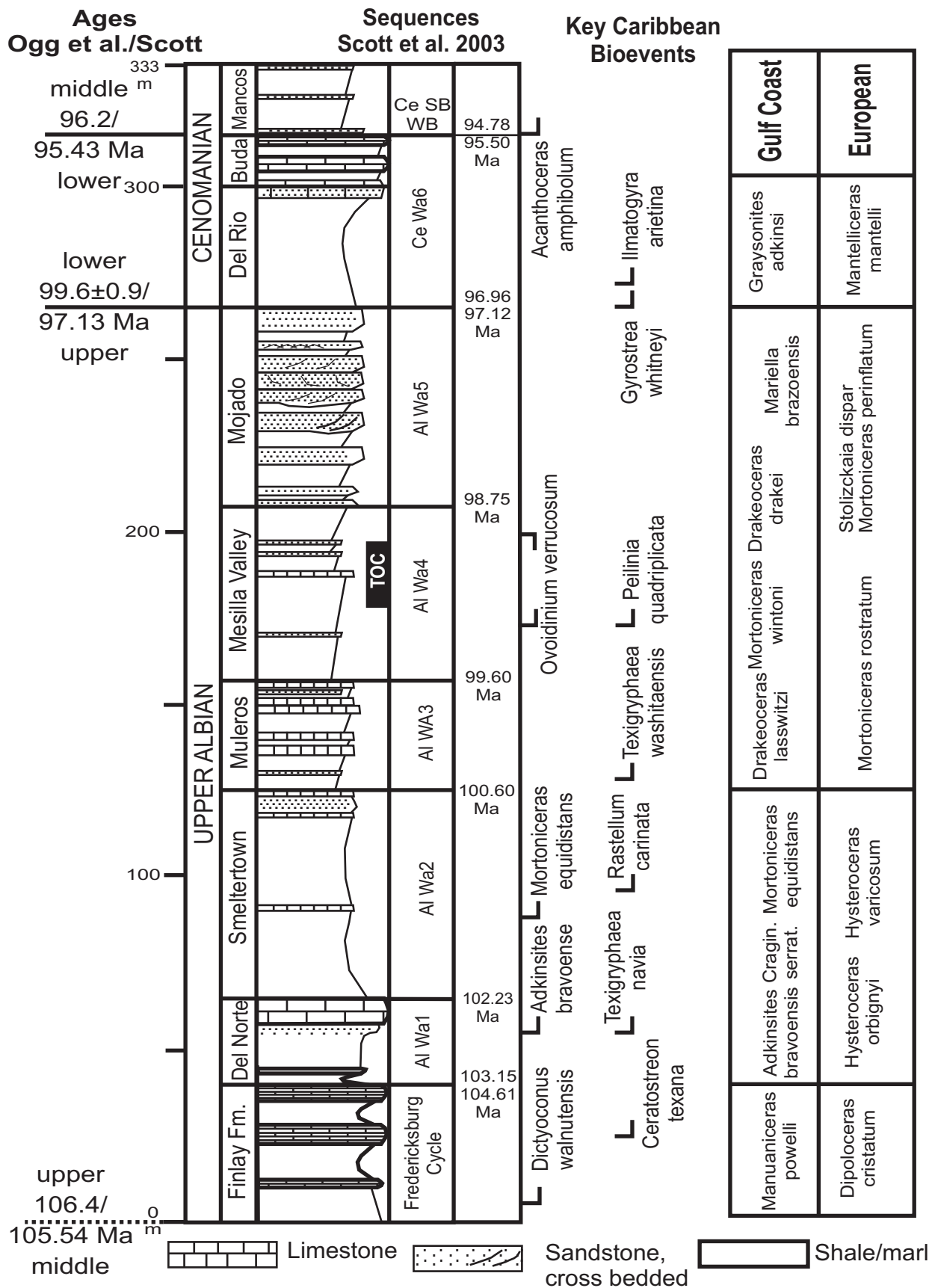


Fig. 3. Stratigraphic section at Cerro de Cristo Rey. Left column numerical age model is from Ogg et al. (2004); lithostratigraphy from Lucas et al. (2010); sequence cycles and age model from Scott et al. (2003); key bioevents composited from various references; Gulf Coast ammonite zones from Kennedy et al. (2005); European ammonite zones from Reboulet et al. (2011) with age model of Scott et al. (2000, 2009).

WA 5. This cycle is calibrated at 98.75–97.03 Ma by graphic correlation with the Cretaceous Chronostratigraphic Database (Scott et al., 2000; Scott, 2009; CRETCSDB at precisionstratigraphy.com) (Fig. 4).

4. Geochemical methods

In order to limit the influence of post-depositional weathering, shale samples were collected by trenching into the slope of the outcrop to expose the more pristine portions of the formation. Samples from the two sample sites were integrated into a complete stratigraphic section for this study (Fig. 5). Kmv 1 samples were collected approximately every 3 m, beginning at the contact between the Muleros and Mesilla Valley formations and continuing up to the contact between the Mesilla Valley and the Mojado Formation. About fifteen meters of section were covered between samples Kmv 1-11 and Kmv 1-12, which was sampled at the second locality. Samples from measured section Kmv 2 were correlated into the measured interval Kmv 1 using the contact between the Mesilla Valley and the Mojado as the stratigraphic datum for correlation. In total 17 shale samples were collected from the Mesilla Valley Formation.

4.1. Total organic and inorganic carbon concentrations

Total carbon (TC) and total organic carbon (TOC) measurements were performed using a Carlo Erba NC500 elemental analyzer. The TOC samples were pretreated with HCl to remove carbonate phases. Total inorganic carbon (TIC) was determined as the difference between TC and TOC.

4.2. Carbon and oxygen isotope ($\delta^{13}\text{C}_{\text{carb}}$, $\delta^{18}\text{O}_{\text{carb}}$) measurement of carbonates

Carbon and oxygen isotope analyses of carbonates were performed at the University of Arkansas Stable Isotope Laboratory. Approximately 0.5 mg of powdered sample was reacted with 105% H_3PO_4 at 25 °C for 18 h to ensure complete reaction of the carbonate and CO_2 headspace equilibration. Samples were then measured using a Thermo Finnigan Delta Plus isotope ratio mass spectrometer coupled to a Thermo Finnigan Conflo-III gas bench. The precision on replicate samples is $\pm 0.1\text{\textperthousand}$.

4.3. Carbon isotope ($\delta^{13}\text{C}_{\text{org}}$) measurement of organic carbon

Powdered samples were analyzed using a Carlo Erba NC 2500 elemental analyzer interfaced to a Thermo Finnigan Delta Plus isotope ratio mass spectrometer. Samples were referenced to a working pure gas, also introduced through the open split. Raw isotope values were normalized to respective scales by the use of certified and in-house standards. Data was further corrected for instrumental drift using standards throughout the run. Three different standards were used for each sample sequence.

4.4. Pyrite sulfur

Determination of the pyrite concentrations, specifically pyrite sulfur (S_{py}), was accomplished through the use of a standard chromium reduction method (Canfield et al., 1986). Briefly, a chromous chloride solution was used to liberate H_2S that is precipitated as zinc sulfide (ZnS), and pyrite concentrations were quantified by micro-titration (Canfield et al., 1986). The titration results quantify S_{py} and Fe_{py} is calculated based on the stoichiometric conversion of pyrite (FeS_2).

4.5. Sequential iron extraction

Sequential iron extractions were performed according to the procedure developed by Poulton and Canfield (2005). The sequential extraction differentiates between iron carbonate minerals (Fe_{carb}), iron oxides (Fe_{ox}), and magnetite (Fe_{mag}). For the sequential iron extraction, the first step is to extract the iron carbonate minerals (Fe_{carb}), such as siderite and ankerite, by reacting the powdered sample with a sodium acetate solution for 48 h. During the second step the remaining sample residue was extracted with sodium dithionite for 2 h to extract iron oxide phases (Fe_{ox}). This was followed by the final extraction step where the residue was extracted with an ammonium oxalate and oxalic acid solution for 24 h to extract magnetite (Fe_{mag}). In between each extraction step, the aliquot solution was diluted with trace-metal-grade 2% HNO_3 and measured on an Agilent 7500ce Inductively Coupled Plasma Mass Spectrometer (ICP-MS).

Highly reactive iron (Fe_{HR}) is calculated by adding the totals from each extraction step to the pyrite iron fraction (Fe_{py}), similar to Poulton and Canfield (2005) and Gill et al. (2011). Fe_{HR} is calculated by summing Fe_{carb} , Fe_{ox} , Fe_{mag} , and Fe_{py} .

4.6. Metal concentrations

Samples were extracted using a multi-acid digestion of trace-metal-clean $\text{HNO}_3/\text{HCl}/\text{HF}$. Following each digestion step the aliquots were combined and evaporated. The samples were then re-dissolved to approximately 5 mL in 2% HNO_3 . This solution was then diluted and analyzed for major (Al, Fe) and minor (Mn) elements on an Agilent 7500ce ICP-MS. Most samples were measured using two isotopes in the optimal mode for that element and analyses had an error of less than 5%. Standard reference materials (USGS SDO-1 and SCO-1 shales) were digested and analyzed with each set of extractions and were within reported errors.

4.7. X-ray diffractometry

X-ray diffraction (XRD) analyses were performed at the University of Tulsa using a Scintag Pad V X-ray Diffractometer and DMSNT controlling software. Powdered samples were scanned from 4 to 65 degrees two-theta, using 0.04-degree steps, and counted for 2.5 s/step. Data were modeled using the Rietveld method and MDI's RIQAS program. Mineral concentrations are normalized to 100%.

5. Results

The geochemical results are reported relative to the depth above the contact between the Muleros and Mesilla Valley formations. The samples were collected at sections 300–800 m northeast of the laccolith contact (Fig. 1) where the thermal alteration index is 3–2 (Norland, 1986, fig. 11). In addition, newly collected in-situ paly-nomorphs are brown not black, indicating that the shale has not been significantly thermally altered.

5.1. Total organic and inorganic carbon

Total organic carbon (TOC) concentrations range from 0.25 to 0.69 wt.% from the base of the Mesilla Valley Formation to near the top of formation (Table 1, Fig. 5). Two trends of increasing concentration are from the base of the section at 0 m to a first maximum at 12.0 m. At a depth of 21.0 m TOC decreases to 0.29 wt.% directly below a sandstone lens. Above this position the most significant increase in TOC throughout the section is up to

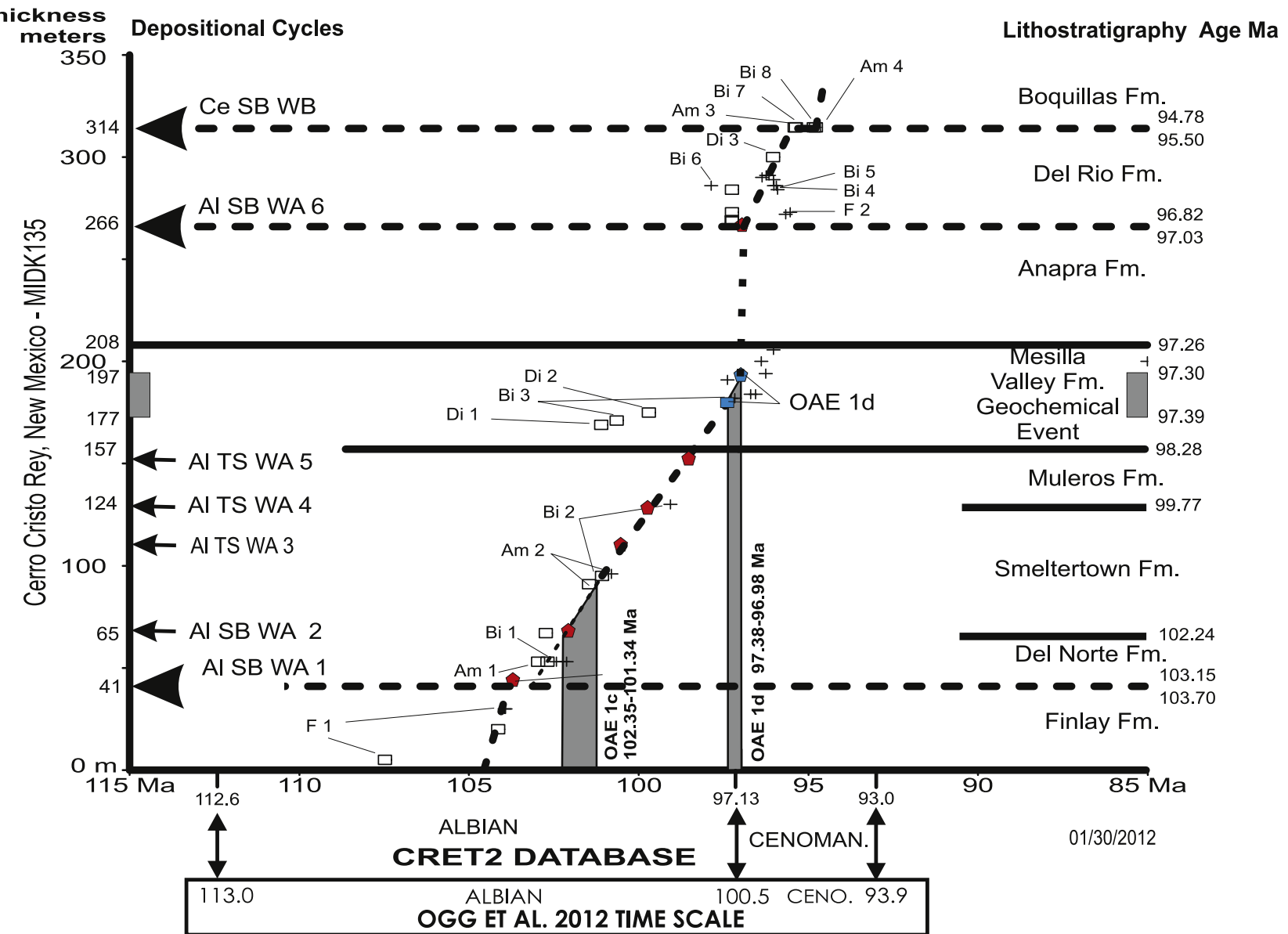


Fig. 4. Chronostratigraphic plot of the Cerro de Cristo Rey Cretaceous section with the global CRET2 Database (Scott, 2009). First appearances are rectangles; last occurrences are plus signs. Solid horizontal lines are depositional contacts; dashed lines are unconformities; dotted lines are correlation hypotheses. Red polygons are boundaries of Washita Group depositional cycles defined in the North Texas section (Scott et al., 2003). The vertical gray bands project into the Cristo Rey section OAEs 1c and 1d defined in deep sea cores and European outcrops. The numerical age model is from Scott (2009) and Scott et al. (2000, 2009; database available at precisionstratigraphy.com). List of key taxa: F1 – *Dictyoconus walnutensis*; F2 – *Cribratina texana*; Am 1 – *Adkinsites bravoensis*; Am 2 – *Mortoniceras equidistans*; Am 3 – *Turritilites acutus*; Am 4 – *Acanthoceras amphibolium*; Bi 1 – *Protocardia texana*; Bi 2 – *Lopha carinata*; Bi 3 – *Pelinia quadruplicata*; Bi 4 – *Ilmatogyra arietina*; Bi 5 – *Exogyra whitneyi*; Bi 6 – *Lopha subovata*; Bi 7 – *Inoceramus arvanus*; Bi 8 – *Ostrea beloiti*; Di 1 – *Hapsocysta dictyota*; Di 2 – *Ovoidinium verrucosum*; Di 3 – *Hystrichosphaeridium tubifera*. (For interpretation of the references to color in this figure legend, the reader referred to the web version of this article.)

Table 1

Geochemical data and sample name.

Sample #	Location	TOC	TIC	$\delta^{13}\text{C}_{\text{TIC-VPDB}}$	$\delta^{13}\text{C}_{\text{TOC-VPDB}}$	$\delta^{18}\text{O}_{\text{VPDB}}$	N _{total}	C/N	S _{py}	Fe _{py}	Fe _{Total}	Fe _{HCl}	Fe _{carb}	Fe _{ox}	Fe _{mag}	Fe _{HR}	Al	Mn
	m	wt%	wt%	‰	‰	‰	wt%	molar	wt%	wt%	wt%	wt%	wt%	wt%	wt%	wt%	wt%	
Kmv 1-14	50.4	0.67			-25.40		0.07	10.55	0.021	0.018	1.91	0.67	0.01	0.58	0.02	0.64	11.33	23.29
Kmv 1-13	49.5	0.61			-24.86		0.08	8.80	0.006	0.005	1.84	0.82	0.01	0.39		0.40	12.18	15.66
Kmv 1-12	48.0																	
Kmv 2-5	43.0	0.59			-25.36		0.09	7.76	0.006	0.005	2.08	0.78	0.02	0.52	0.02	0.55	11.10	58.97
Kmv 2-4	40.0	0.69			-24.80		0.09	8.97	0.004	0.003	2.64	1.18	0.01	0.82	0.06	0.90	10.97	14.08
Kmv 2-3	37.0	0.69			-25.67		0.08	9.81	0.003	0.003	2.82	1.31	0.02	0.55	0.08	0.65	11.32	120.11
Kmv 2-2	34.0	0.63	0.09	-2.91	-25.46	-1.16	0.12	6.19	0.007	0.006	4.13	2.46	0.04	0.94	0.24	1.23	11.10	335.71
Kmv 2-1	31.0	0.51	0.11	-2.35	-25.74	-2.60	0.08	7.86	0.006	0.005	3.41	1.88	0.04	1.04	0.16	1.24	10.33	159.79
Kmv 1-11	30.0	0.63	0.06	-1.80	-25.51	-2.82	0.07	10.99	0.006	0.005	3.51	3.28	0.05	1.25	0.14	1.44	11.03	113.91
Kmv 1-10	27.0	0.52	0.8	-2.37	-25.74	-7.57	0.08	7.43	0.019	0.016	2.43	4.56	0.07	1.26	1.27	2.61	8.95	17.70
Kmv 1-9	24.0	0.38	1.14	-2.49	-25.63	-7.27	0.08	5.78	0.009	0.008	4.10	3.26	0.06	1.01	0.21	1.28	8.64	188.35
Kmv 1-8	21.0	0.29	0.69	-2.48	-26.41	-7.63	0.07	4.83	0.007	0.006		1.98	0.09	0.46	0.24	0.79		
Kmv 1-7	18.0	0.50	0.09	-2.05	-26.09	-4.66	0.09	6.53	0.006	0.005	3.16	1.87	0.05	0.66	0.05	0.76	10.45	72.98
Kmv 1-6	15.0																	
Kmv 1-5	12.0	0.55			-26.16		0.08	8.05	0.010	0.009	4.27	2.66	0.07	0.92	0.22	1.22	10.06	131.07
Kmv 1-4	9.0	0.55	0.35	-2.08	-25.87	-6.95	0.08	7.89	0.023	0.020	3.47	2.46	0.08	1.28	0.15	1.53	10.84	133.55
Kmv 1-3	6.0	0.50	1.02	-2.19	-26.13	-8.04	0.07	8.21	0.010	0.008	4.84	3.70	0.07	1.74	0.16	1.99	8.49	249.01
Kmv 1-2	3.0	0.42	1.25	-2.57	-25.67	-9.22	0.06	8.22	0.009	0.008	2.75	2.08	0.12	0.79	0.05	0.96	6.87	260.68
Kmv 1-1	0.0	0.25	2.16	-2.23	-26.37	-8.10	0.05	6.17	0.005	0.004	2.52	1.86	0.12	0.61	0.05	0.78	5.56	161.63

TOC = total organic carbon.

TIC = total inorganic carbon.

HCl = unsulfidized reactive iron.

carb = iron carbonate minerals.

ox = iron oxides (goethite, hematite, etc.).

mag = magnetite.

HR = highly reactive iron.

Fe_{HR} = Fe_{py} + Fe_{carb} + Fe_{ox} + Fe_{mag} (Gill et al., 2011).

0.40 wt.% from 21.0 to 40.0 m, which is the interval of the proposed OAE.

The $\delta^{13}\text{C}_{\text{organic}}$ values are reported relative to V-PDB. Values are relatively consistent throughout the section and range from -26.41 to -24.80‰ (Table 1, Fig. 5). These enriched values occur in a specific stratigraphic zone from approximately 21.0 to 40.0 m and represent a positive $\delta^{13}\text{C}$ shift of +1.6‰.

Total inorganic carbon (TIC) concentrations decrease from 2.16 wt.% to 0.09 wt.% over the depth interval from 0.0 to 18.0 m, however, at 12.0 and 15.0 m depths concentrations of TIC were not measureable (Table 1, Fig. 5). TIC increases to a maximum concentration of 1.14 wt.% at 24.0 m, followed by an abrupt decrease to concentrations between 0.06 and 0.11 wt.%. The increase between 18.0 and 24.0 m corresponds to a decrease in TOC followed by an increase. Concentrations are below the detection limit above 34.0 m.

The $\delta^{13}\text{C}_{\text{inorganic}}$ values are reported relative to V-PDB and range from -2.91 to -1.80‰ (Table 1, Fig. 5). A positive $\delta^{13}\text{C}$ shift of approximately +0.7‰ is from 21.0 to 30.0 m, followed by a depletion and negative -1.1‰ shift from 30.0 to 34.0 m. Above 34.0 m $\delta^{13}\text{C}$ could not be measured.

The $\delta^{18}\text{O}_{\text{carbonate}}$ ranges from -9.22‰ to -1.16‰ relative to V-PDB from the base of the Mesilla Valley Formation to the top sample at 34.0 m (Table 1, Fig. 5). Due to the coarse resolution of samples, a result of the low TIC concentrations, it is not possible to determine detailed isotope trends. However, two regions of ^{18}O enrichments occur from 3.0 to 18.0 m (+4.56‰) and from 27.0 to 34.0 m (+6.41‰). At approximately 21.0 m a negative excursion is from -4.66‰ to -7.63‰.

5.2. Pyrite concentrations

Pyrite-S (S_{py}) concentrations are low and range from 0.003 to 0.023 wt.% in the Mesilla Valley (Table 1, Fig. 6). Three concentration maxima are located at 9.0, 27.0 and 50.4 m with concentrations reaching 0.023 wt.%. Between these maxima are extended periods

of background S_{py} concentrations that are relatively constant and lower, ranging between 0.003 and 0.010 wt.% S_{py}. Overall, the maximum S_{py} concentrations are low throughout the Mesilla Valley.

5.3. Sequential iron extractions

The sequential iron extraction data show that Fe_{carb} concentrations are low throughout the entire section and do not exceed 0.12 wt.% (Table 1, Fig. 6). Fe_{ox} concentrations range from 0.39 to 1.74 wt.% with maximum concentrations occurring from 6.0 to 9.0 m and 24.0 to 34.0 m. Fe_{mag} concentrations are also relatively low with the majority of sample concentrations ranging from 0.05 to 0.24 except for a maximum value of 1.27 wt.% at 27.0 m.

Concentrations of Fe_{HR} are determined by taking the sum of Fe_{py} + Fe_{carb} + Fe_{ox} + Fe_{mag} as previously described. These concentrations range from 0.40 to 2.61 wt.% throughout the Mesilla Valley Formation. Maximum concentrations occur between 6.0–12.0 m and 24.0–34.0 m.

Total Fe, Fe_T concentrations range from 1.84 to 5.86 wt.% in the Mesilla Valley. Concentrations of Fe_T are higher between the depths from 0.0 to 43.0 m than above, with maxima values of 4.84 wt.% at 6.0 m and 5.86 wt.% at 27.0 m. Values tend to remain elevated between 18 m and 27 m, culminating in the maximum at 27.0 m. These concentrations decrease above this horizon and lower concentrations are measured in the upper section of the Mesilla Valley.

Low ratios of Fe_{py}/Fe_{HR} occur throughout the section. Fe_T/Al ratios tend to remain below Post-Archaean Average Australian Shale values (PAAS) of 0.5 except at 6.0 and 27.0 m, where values show minor iron enrichments. Fe_{HR}/Fe_T ratios exceed the 0.38 threshold for anoxic conditions (Anderson and Raiswell, 2004; März et al., 2008) at 6.0, 9.0, 27.0 and 30.0 m depths. Two enrichment trends precede these elevated values. The first begins at the base of the Mesilla Valley Formation and the second begins at 18.0 m. Coupled to the Fe_{HR}/Fe_T ratios, the Fe_{py}/Fe_{HR} ratios are all very low (0.00–0.03) throughout the entire Mesilla Valley.

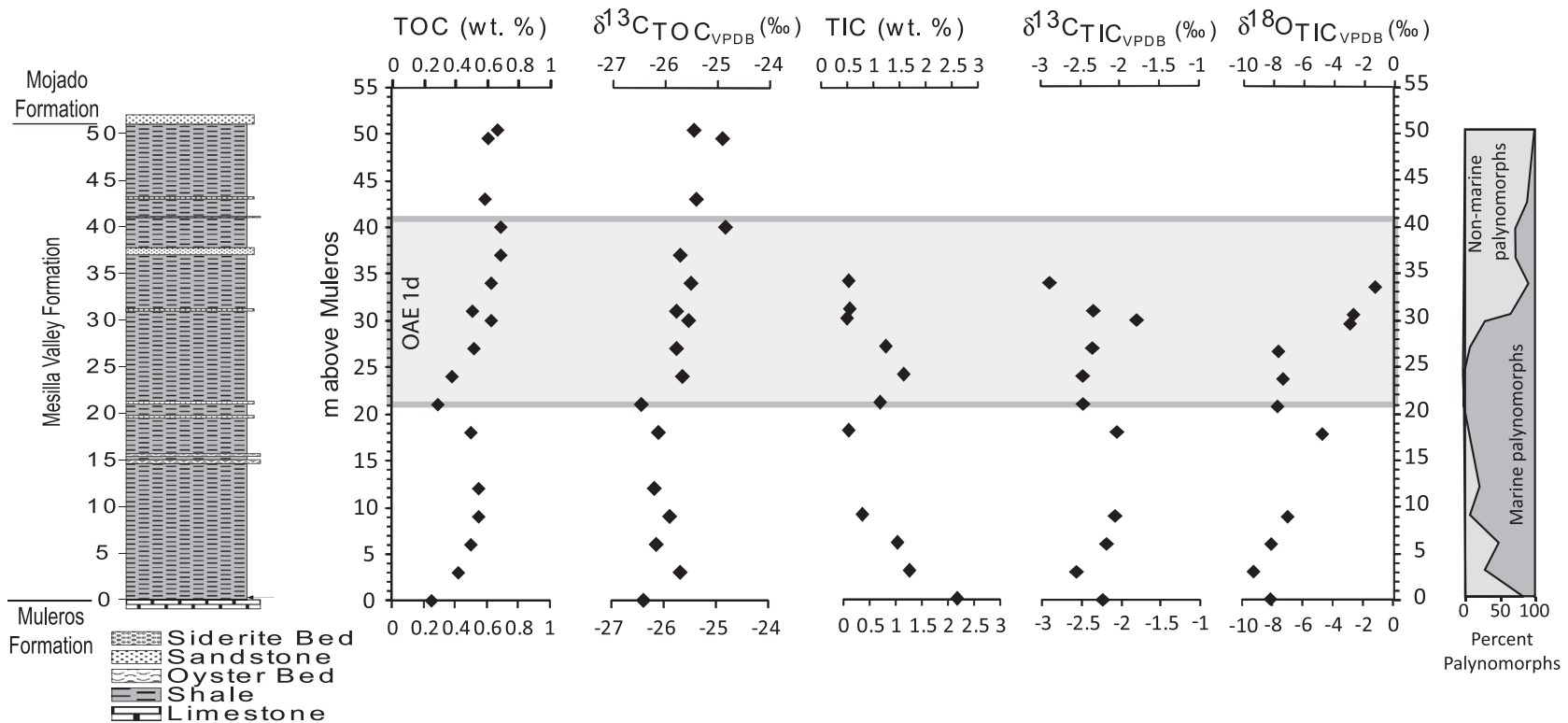


Fig. 5. Total organic carbon (TOC) and inorganic carbon (TIC) concentration and $\delta^{13}\text{C}$ and $\delta^{18}\text{O}$ results. The identified OAE 1d section is outlined by the gray box and occurs approximately between 21 and 40 m.

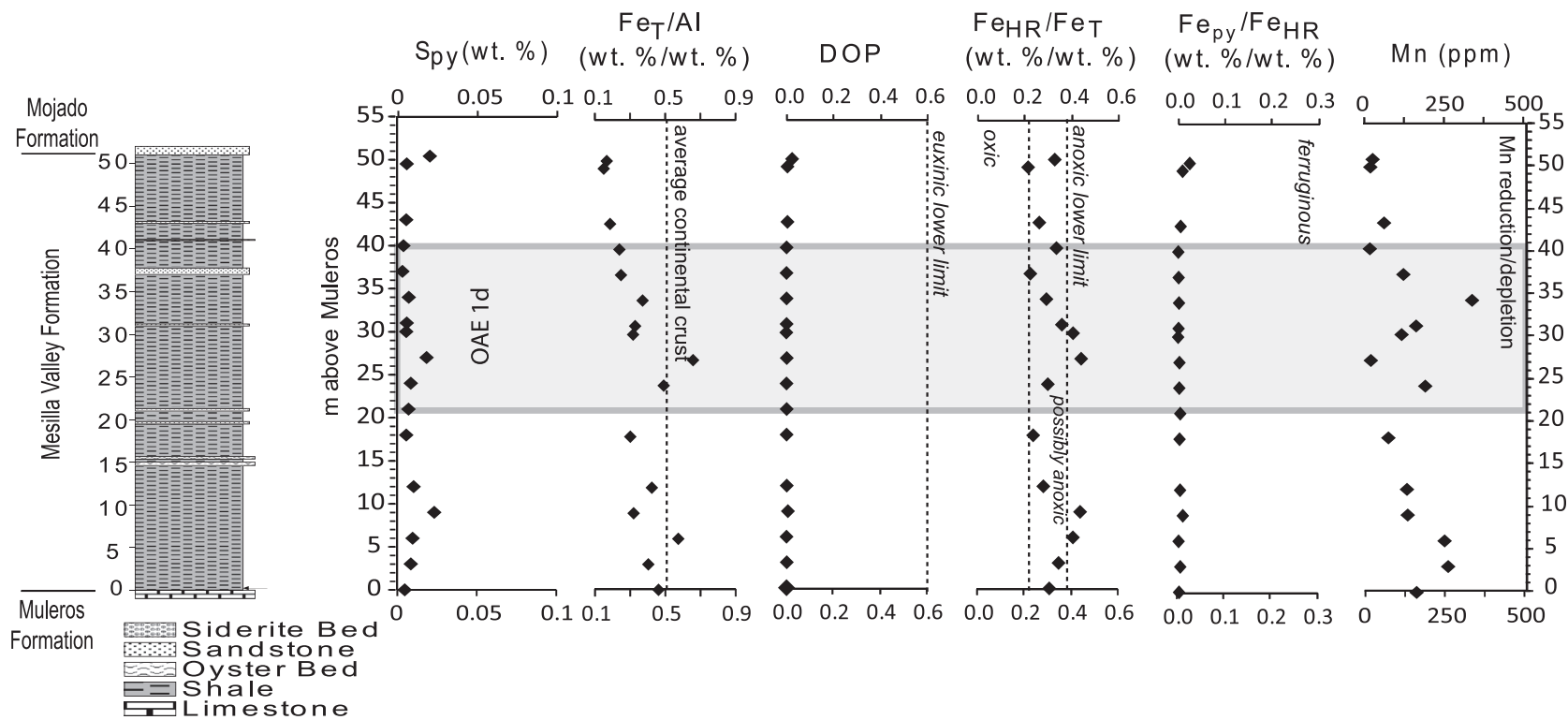


Fig. 6. Sequential iron data, pyrite concentrations (S_{py}) and manganese concentrations. The identified OAE 1d section is outlined by the gray box and occurs approximately between 21 and 40 m.

5.4. Major and minor elements

A suite of major and minor elements was measured in this study and of particular interest are the concentrations of Fe, Al and Mn. Manganese concentrations range between 17.7 and 335.7 ppm throughout the section (Table 1, Fig. 6). These values are below the average crustal PAAS value of 850 ppm (Taylor and McLennan, 1985) and the North American Shale Composite (NASC) average of 465 ppm (Gromet et al., 1984). Overall, there were no major observed enrichments in other trace metals. Total iron concentration results are provided in Section 5.3.

6. Discussion

6.1. Definition of OAE 1d interval in the Mesilla Valley Formation

A multi-proxy geochemical study based on low-resolution sampling and constrained by a biostratigraphic framework was utilized to identify OAE 1d in the upper part of the Mesilla Valley Formation. Geochemical signatures of OAEs are enrichment in TOC concentrations coupled with positive $\delta^{13}\text{C}$ excursions (e.g. Schlanger and Jenkyns, 1976; Scholle and Arthur, 1980; Jenkyns and Wilson, 1999; Kuypers et al., 2002; Herre et al., 2004; Jenkyns, 2010). The carbon isotope shift of major Cretaceous OAEs is on the order of +1.5‰ or greater (Herre et al., 2004; Bornemann et al., 2005). TOC concentrations of the Mesilla Valley range from a low of 0.25 wt.% at the base of the formation to a maximum of 0.69 wt.% at the top. Specifically from 21.0 m to 40.0 m TOC increases to approximately 0.40 wt.%. In this same stratigraphic interval the $\delta^{13}\text{C}_{\text{org}}$ positive excursion is +1.6‰ (Fig. 5).

The organic matter in the Mesilla Valley Formation is type III, indicating a terrigenous source (Belle, 1987). Consistent with this previous work, the $\delta^{13}\text{C}_{\text{org}}$ values range from -26.4 to -24.8‰, which are close to the average end-member of C3 plants at -27.0‰. Modern marine organic matter averages -20.0‰. On average, the source of the organic matter, based on these results, is terrestrial with varying amounts of marine organic matter. Although the natural variability in the $\delta^{13}\text{C}_{\text{org}}$ precludes a more precise determination of the relative amounts of terrestrial or marine organic matter, C/N ratios and palynomorph data more accurately track the variations in source. The C/N molar ratios are also clues to the depositional dynamics and organic matter sources (Meyers, 1994; Gilhooly et al., 2008). C/N ratios of marine organic matter are typically lower (4–10) than that of terrestrial organic matter (>20) (Emerson and Hedges, 1988; Meyers, 1997; Boulobassi et al., 1999). Following the approach of Gilhooly et al. (2008), we utilized a simple mass balance calculation to quantify the variability in terrestrial and marine organic matter inputs. For our calculations the C/N ratio end-member for marine organic matter is 4.8, close to the Gilhooly et al. (2008) value and within the values presented by Meyers (1994). The terrestrial end-member C/N ratio for the calculation is 20. Results are compared with palynomorph data (Fig. 5). Both the C/N isotope mass balance and the palynomorph data show increasing deposition and/or preservation of marine organic matter up section from 0.0 to 21.0 m. Above 21 m the amount of terrestrial organic matter increases up-section. The enrichment also corresponds to the slight enrichment in $\delta^{13}\text{C}_{\text{org}}$, which would be expected with increased marine organic matter inputs, but the bulk $\delta^{13}\text{C}_{\text{org}}$ values remain indicative of a dominantly terrestrial source of organic matter. Overall, these data show that marine organic matter increases up to the middle part of the section and in the upper part it was overwhelmed by terrestrial input.

Associated with the start of the positive $\delta^{13}\text{C}_{\text{org}}$ excursion above 21 m is a negative excursion in $\delta^{13}\text{C}_{\text{TIC}}$ and $\delta^{18}\text{O}_{\text{TIC}}$. Both $\delta^{13}\text{C}_{\text{TIC}}$ and

$\delta^{18}\text{O}_{\text{TIC}}$ exhibit a positive excursion in the middle of the assigned OAE 1d event (Fig. 5). The utility of this isotope record is dependent on the level of post-depositional diagenetic alteration. A simple plot of $\delta^{13}\text{C}_{\text{TIC}}$ vs $\delta^{18}\text{O}_{\text{TIC}}$ indicates no correlation ($R^2 = 0.002$) suggesting no major post-depositional diagenetic, thermal or tectonic overprint of these carbonates. This conclusion is supported by positive carbon and negative oxygen isotope values of limestone in the underlying Finlay Formation that are similar to values of coeval subsurface formations, and that do not plot as “inverted J” or “inverted T” patterns indicative of exposure to meteoric waters (Railsback et al., 2003; Rush, 2012). In addition, carbonate matrix petrography shows little diagenetic effects although fractures are filled with secondary calcite. Carbonate minerals in the Mesilla Valley Formation are less than ten percent, and the negative inorganic carbon isotope values of -1.7 to -3‰ suggest minor diagenetic effects. The negative $\delta^{18}\text{O}_{\text{TIC}}$ values are in the range of typical Lower Cretaceous limestone in the Gulf coast that has not been exposed to meteoric conditions (Rush, 2012).

Also, concurrent with the $\delta^{13}\text{C}$ positive excursions is a negative $\delta^{18}\text{O}$ excursion in the TIC. It has been suggested that OAEs can be related to thermal maxima (Jenkyns et al., 1994; Wilson and Norris, 2001; Voigt et al., 2006; Jenkyns, 2010). The sample at 21.0 m in the Mesilla Valley section shows an abrupt negative excursion. This could indicate an increase in water temperature (Friedman and O’Neil, 1977), which may be recorded in the inorganic carbon pool. The $\delta^{13}\text{C}_{\text{TIC}}$ may be recording an initial shift in the carbon isotope fraction associated with the re-mineralization of more ^{13}C -depleted organic matter, followed by enrichment in $\delta^{13}\text{C}_{\text{TIC}}$ as organic carbon burial increased. Similar temporal divergence between $\delta^{13}\text{C}_{\text{TIC}}$ and $\delta^{13}\text{C}_{\text{org}}$ has been observed in other Cretaceous OAE sections, specifically the early Albian (Menegatti et al., 1998). The continued enrichment in ^{18}O during the 1d event may be indicative of a sea-level fall (for review see Föllmi, 2012). Relative sea-level fall is also indicated by the gradation of the Mesilla Valley shale into shoreface sandstone of the Mojado Formation. When this is considered, the data are in concert with TOC and $\delta^{13}\text{C}_{\text{TOC}}$ enrichments indicative of OAE 1d.

6.2. Iron geochemistry and Mn results

Iron geochemical proxies provide a fingerprint to distinguish paleoredox conditions (Fig. 6). Overall, reactive iron is typically enriched under protracted anoxic, and particularly euxinic, conditions. These enrichments are recorded as elevated $\text{Fe}_{\text{HR}}/\text{Fe}_{\text{T}}$ and $\text{Fe}_{\text{T}}/\text{Al}$ ratios (Lyons and Severmann, 2006). $\text{Fe}_{\text{T}}/\text{Al}$ ratios for average continental crust are approximately 0.5 (Taylor and McLennan, 1985) and enrichments above this value indicate a degree of iron-enrichment in the sediments. Pulses of mild iron enrichments are seen at depths of 6.0 and 27.0 m; the latter is associated with the assigned OAE 1d horizon in the Mesilla Valley Formation (Fig. 6). Fe enrichment mechanisms can be highlighted with additional iron ratios. The generalized $\text{Fe}_{\text{HR}}/\text{Fe}_{\text{T}}$ threshold for anoxia is 0.38 (Raiswell and Canfield, 1998; Poulton and Raiswell, 2002). Four depths, 6.0, 9.0, 27.0 and 30.0 m, exhibit enrichments greater than this 0.38 threshold suggesting these samples were deposited under anoxic conditions. The majority of the remaining depths have ratios that fall between 0.22 and 0.38, indicative of sediments deposited under ‘normal’ marine conditions, but when considered with additional geochemical data, suggest that anoxic or low oxygen conditions were plausible (see discussion below). The samples at 27.0 and 30.0 m correspond with the OAE at this section.

Poulton and Raiswell (2002) also determined that on average, ancient sediments that have been deposited under oxic conditions have $\text{Fe}_{\text{HR}}/\text{Fe}_{\text{T}}$ of 0.14 ± 0.08 , which are lower than the anoxic threshold used in this study and the majority of the data. In

addition, when using the most elevated oxic $\text{Fe}_{\text{HR}}/\text{Fe}_T$ ratio ≤ 0.22 it is possible to categorize $\text{Fe}_{\text{HR}}/\text{Fe}_T$ values between 0.22 and 0.38, as likely anoxic deposition. While a majority of the $\text{Fe}_{\text{HR}}/\text{Fe}_T$ values do fall in the intermediate range, deposition was likely in anoxic waters with water column iron enrichments being masked by rapid sedimentation (Raiswell and Canfield, 1998). Based on a total formation thickness of 51 m deposited over 1.2 myr, the average sedimentation accumulation rate for the Mesilla Valley Formation was extremely rapid and approximately 42.5 m/myr. These conditions could have muted further enrichment of the $\text{Fe}_{\text{HR}}/\text{Fe}_T$ ratios due to dilution by increased terrestrial sedimentation, which would retard a possible Fe shuttle. Werne et al. (2002) reported a similar mechanism from the Middle Devonian Oatka Creek Formation.

The use of $\text{Fe}_{\text{HR}}/\text{Fe}_T$ ratios can indicate anoxic conditions but cannot distinguish between euxinic or ferruginous conditions. However, the $\text{Fe}_{\text{py}}/\text{Fe}_T$ ratio is effective at defining these conditions. The ratios of $\text{Fe}_{\text{HR}}/\text{Fe}_T$ of four samples plot within the anoxic zone. All other samples from the Mesilla Valley Formation plot within $\text{Fe}_{\text{py}}/\text{Fe}_{\text{HR}}$ ratios indicative of ferruginous conditions ($\text{Fe}_{\text{py}}/\text{Fe}_{\text{HR}} < 0.7$; Fig. 6), indicating an iron-rich depositional environment in which unsulfidized iron is present as ferric (oxyhydr) oxides (e.g. ferrihydrite) and/or ferrous carbonates (e.g., siderite).

Pyrite is scarce throughout the section, further corroborating the persistence of ferruginous and anoxic conditions and that euxinic conditions were rare, or non-existent, during OAE 1d at this site. The slight enrichments in Fe_T/Al and $\text{Fe}_{\text{HR}}/\text{Fe}_T$, along with no enrichments in $\text{Fe}_{\text{py}}/\text{Fe}_{\text{HR}}$ indicate that the interval associated with OAE 1d in the Mesilla Valley Formation was deposited in an iron-rich, anoxic environment, nearly devoid of dissolved sulfide. The relationships among the Fe species are consistent with the expansion of low-oxygen conditions in shallow marine environments with high sedimentation rates that may dilute organic carbon enrichment and suppress elevated sulfate reduction rates (and therefore the availability of sulfide). This environment also provides a consistent source of clastic detrital iron minerals. Additionally, if these sediments remain dysoxic, they may be a source of dissolved iron to the overlying water-column or to other sediments (Severmann et al., 2008; Lyons et al., 2009).

In addition to carbon-iron geochemical signatures, manganese trace metal concentrations in the Mesilla Valley Formation also provide insights regarding the depositional redox conditions. The concentrations of sedimentary Mn are often depleted under dysoxic and anoxic conditions. Mn-reduction in the sediments results in a flux of dissolved Mn out of the sediments into the overlying low- O_2 water (Calvert and Pedersen, 1992; Morford and Emerson, 1999). Mn concentrations in the entire Mesilla Valley section are depleted below the Post-Archaean Average Shale (PAAS) baseline of 850 ppm (Taylor and McLennan, 1985) and below the North American Shale Composite (NASC) average of 465 ppm (Gromet et al., 1984) (Fig. 6). The strongest depletions are associated with the onset and termination of the OAE 1d in this section. The paleoredox conditions during the deposition of the Mesilla Valley, and specifically OAE 1d, must have been dysoxic to anoxic. This is consistent with the lack of sulfide minerals and measured Mn concentrations in this section. The presence of Fe enrichments recorded in Fe_T/Al and $\text{Fe}_{\text{HR}}/\text{Fe}_T$, with the lack of $\text{Fe}_{\text{py}}/\text{Fe}_{\text{HR}}$ and pyrite enrichments, associated with the Mn depletions suggests that the Mesilla Valley was dominated by anoxic and Fe-rich conditions during the time period associated with OAE 1d.

6.3. Definitions of Late Albian OAEs and correlation of Mesilla Valley with OAE 1d

Cretaceous oceanic anoxic events resulted from the interaction of multiple factors including warming temperatures due to abrupt

rise of atmospheric CO_2 , more intense continental weathering, high runoff, and greater nutrient input, which together with upwelling increased marine productivity (Jenkyns, 2010).

Two widespread late Albian anoxic events, OAE 1c and OAE 1d, are defined by sets of thin black, organic-rich shale interbedded with marl and by positive carbon isotope excursions (Leckie et al., 2002; Ogg et al., 2004; Coccioni et al., 2012). Oceanic Anoxic Event 1c is an early late Albian event spanning the *Biticinensis breggiensis* Zone/*Thalmanninella praeticinensis* to *Pseudothalmanninella subticinensis* Subzones and *Axopodorhabdus albianus* Zone NC9B (Bralower et al., 1993; Leckie et al., 2002; Coccioni et al., 2012). The Amadeus segment of the Scisti a Fucoidi Formation in central Italy is part of OAE 1c (Coccioni and Galeotti, 1993; Galeotti et al., 2003). The Toolebuc Formation in NE Australia also records OAE 1c (Haig and Lynch, 1993). Bralower et al. (1993) assigned OAE 1c to TOC peaks at DSDP Site 370 in the Morroco Basin, Site 258 in the Naturaliste Plateau, Indian Ocean, and Site 400 in the Bay of Biscay. Terrestrial organic matter resulting from high sedimentation during maximum sea-level fall dominates OAE 1c black shales (Haq et al., 1987; Erbacher et al., 1996; Erbacher and Thurow, 1997). No pelagic extinction event was associated with OAE 1c (Erbacher and Thurow, 1997; Leckie et al., 2002).

Oceanic Anoxic Event 1d is a latest late Albian event spanning the *Parathalmanninella appenninica/Planomalina buxtorfi* Zone and the *Eiffellithus turrisieffelii* Zone NC10 (Leckie et al., 2002; Ogg et al., 2012; Coccioni et al., 2012). The typical black organic-rich shale interval is the Breistroffer bed in southern France (Bréhéret and Delamette, 1989; Bréhéret, 1997; Erbacher et al., 1996; Wilson and Norris, 2001; Leckie et al., 2002). OAE 1d is composed of up to 3.5% marine organic matter associated with a carbon isotope shift of 0.5–2‰ and pelagic biotic turnover events (Leckie et al., 2002). This event has been identified at ODP Site 1052 in the western Atlantic Blake Nose, at DSDP Site 545 offshore Morocco, at the Mont Risou Cenomanian GSSP section in southern France (Herrelle et al., 2004; Kennedy et al., 2004; Gale et al., 2011), and at Roter Sattel, Switzerland (Strasser et al., 2001) as well as in the southern Indian and eastern Pacific oceans (Leckie et al., 2002). OAE 1d is associated with planktic extinction and radiation events (Erbacher et al., 1996; Leckie et al., 2002) that suggest major oceanic environmental changes such as collapse of the water mass stratification.

At Mont Risou, France, OAE 1d is recorded in the Breistroffer bed, which is a set of thin, organic-rich beds interbedded with pelagic marl (Gale et al., 1996, 2011). Four positive shifts of about 0.5‰ in $\delta^{13}\text{C}_{\text{carb}}$ compose the Albian–Cenomanian boundary event (Jarvis et al., 2006; Gale et al., 2011). This event apparently was driven by climatic cycles that increased marine productivity; it is associated with high turnover in marine biota. In contrast to these oceanic pelagic basins, the organic-rich, anoxic signal in the Mesilla Valley Formation was deposited close to shore and was strongly affected by terrigenous runoff and high rates of sediment accumulation (~40 m/myr). This is approximately four times faster than average oceanic pelagic deposits (Scott, 2009).

Chronostratigraphic and biostratigraphic evidence supports the interpretation of the presence and timing of OAE 1d in the Mesilla Valley Formation. The chronostratigraphic age of the geochemical event in the Mesilla Valley Formation is latest Albian 97.39–97.30 Ma (Fig. 4). This age is derived by comparing the biostratigraphic and sequence stratigraphic events at Cerro de Cristo Rey with these events in the global CRET2 database (Scott et al., 2001; the next developmental stage is CRETCSDB1, which spans all Cretaceous stages documented at: precisionstratigraphy.com). Published ages of OAE 1d/Breistroffer bed vary; Leckie et al. (2002) estimated the age at ~99.5 Ma and Ogg et al. (2012, fig. 27.6) projected the age at 101 Ma. Ages of the CRETCSDB1 global

database are projected into the Cerro de Cristo Rey section by the line of correlation (LOC), which is constrained by the first and last occurrences (FO-rectangles; LO-plus signs) of ammonites, bivalves, dinoflagellates, and depositional cycle boundaries (Fig. 4). The FOs of *Ovoidinium verrucosum* (99.70–95.95 Ma) and *Hapso-cysta dictyota* Davey (101.11–94.64 Ma) are above the LOC because the lower part of the section has not been sampled for dinoflagellates. A cluster of LOs of bivalves and dinoflagellates in the upper part of the Mesilla Valley brackets the LOC. The bases of shale-limestone depositional cycles defined in the North Texas section (Scott et al., 2003) also constrain the LOC. Transgressive-regressive cycle Al WA5 is the base of the dark gray shale Pawpaw Formation that underlies the prograding Main Street Formation in North Texas and correlates with the base of the Mesilla Valley. The two late Albian OAEs, 1c and 1d, are positioned into the CRET2 and CRETCSDB1 from oceanic cores and outcrop reference sections (DSDP 386, 400A, 545, and outcrop sections at Gubbio, Italy, Mont Risou, France, Roter Satel, Switzerland, and Coppa Nuvolla, Italy). As defined in these sections OAE 1c is dated at 102.35–101.39 Ma, which correlates with the *Biticinella breg-giensis* and *Mortoniceras inflatum* zones, and OAE 1d is dated at 97.38–96.98 Ma, which correlates with the *Parathalmanninella appenninica* and the *Stoliczkaia dispar* zones. When integrated with biostratigraphic and temporal graphic correlation, the geochemical event in the Mesilla Valley is latest Albian and can be identified as OAE 1d.

7. Conclusions

The Mesilla Valley Formation was deposited on a prograding terrigenous shelf close to land during shore progradation. Terrestrial kerogens, moderate isotope excursions and geochemical trends suggest that OAE 1d is recorded in the Mesilla Valley and was influenced by high detrital input similar to the Detrital-OAE model (Erbacher et al., 1996) in contrast to oceanic pelagic deposits of OAE 1d. The geochemical data suggest that bottom waters would have been dysaerobic to anoxic, but not euxinic, and ferruginous conditions were consistent with a reduced oxygen minimum zone (OMZ). Enriched iron ratios that temporally correlate with Mn depletions and other traditional geochemical evidence of OAEs, including increasing TOC concentrations and carbon isotope excursions, provide a systematic framework to recognize OAE 1d in the Mesilla Valley section. The Mesilla Valley geochemical event is latest Albian and can be identified as OAE 1d.

Chronostratigraphic and biostratigraphic evidence confirms that the Mesilla Valley Formation is the appropriate age to have been deposited during OAE 1d. Enrichments in $\delta^{13}\text{C}_{\text{TOC}}$, the presence of Fe enrichments recorded in Fe_T/Al and $\text{Fe}_{\text{HR}}/\text{Fe}_T$ with the lack of $\text{Fe}_{\text{py}}/\text{Fe}_{\text{HR}}$ and degree-of-pyritization enrichments associated with Mn depletions suggest that the Mesilla Valley sediments were deposited under low oxygen to anoxic and at times Fe-rich, conditions during deposition. In addition, the combination of these data suggests that OAE 1d in this basin was deposited under high rates of terrigenous sediment input during shoreline progradation. This detrital-dominated OAE in anoxic bottom waters differs from records of OAE 1d in the Atlantic and Mediterranean basins, which are dominated by high marine productivity and anoxia. The differences between these depositional regimes are recorded by the geochemical signatures preserved in the Mesilla Valley section. Thus, by integrating these independent lines of evidence we have been able to recognize this type of OAE. A more closely spaced sampling program would define the isotope excursions and geochemical trends with greater confidence.

Acknowledgments

The authors would like to thank Erik Pollock and Lindsey Conaway from the University of Arkansas Stable Isotope Laboratory for their assistance with the stable isotope analyses. We would also like to thank Steve Bates from the University of California-Riverside for help with the trace metal measurements. Also, we are grateful to Dr. Winton Cornell for help during the sampling and interpretation of these sections. We would like to acknowledge the financial support from the University of Tulsa Student Research Grant Program to N. Rush, funding from AAPG (Frank Kottlowski fund to N. Rush) and Precision Stratigraphy Associates (Tulsa, OK).

References

- Anderson, T.F., Raiswell, R., 2004. Sources and mechanisms for the enrichment of highly reactive iron in euxinic Black Sea sediments. *American Journal of Science* 304, 203–233.
- Arnaud-Vanneau, A., Bilotte, M., 1998. Larger benthic foraminifera. In: de Granciansky, P.-C., Hardenbol, J., Jacquian, Th., Vail, P.R. (Eds.), Mesozoic–Cenozoic sequence stratigraphy of European Basin, SEPM (Society for Sedimentary Geology) Special Publication No. 60, pp. 772–773 (chart 5).
- Arthur, M.A., Brumsack, H.-J., Jenkyns, H.C., Schlanger, S.O., 1990. Stratigraphy, geochemistry, and paleoceanography of organic carbon-rich Cretaceous sequence. In: Ginsburg, R.N., Beaudoin, B. (Eds.), Cretaceous Resources, Events and Rhythms. Kluwer Academic, pp. 75–119.
- Arthur, M.A., Dean, W.E., Schlanger, S.O., 1985. Variations in the global carbon cycle during the Cretaceous related to climate, volcanism, and changes in atmospheric CO_2 . In: Sundquist, E.T., Broecker, W.S. (Eds.), The carbon cycle and atmospheric CO_2 : Natural variations Archean to present, Geophysical Monograph 32. American Geophysical Union, pp. 504–529.
- Belle, E.R., 1987. A geochemical study of the organic matter within the Lower Cretaceous Mesilla Valley shale, Cerro de Cristo Rey uplift, Doña Ana County, New Mexico. The University of Texas at El Paso, El Paso, TX, 111 p. (MSc. thesis).
- Bornemann, A., Pross, J., Reichelt, K., Herrle, J.O., Hemleben, C., Mutterlose, J., 2005. Reconstruction of short-term palaeoceanographic changes during the formation of the Late Albian 'Niveau Breistroffer' black shales (oceanic anoxic event 1d, SE France). *Journal of the Geological Society, London* 162, 623–639.
- Böse, E., 1910. Monografía geológica y paleontológica del Cerro de Muleros cerca de Ciudad Juárez, Estado de Chihuahua, y descripción de la fauna cretacea de La Encanatada, Placer de Guadalupe, Estado de Chihuahua. Instituto Geológico de México, Bulletin 25, 193.
- Bouloubassi, I., Rullkötter, J., Meyers, P.A., 1999. Origin and transformation of organic matter in Pliocene-Pleistocene Mediterranean sapropels: organic geochemical evidence reviewed. *Marine Geology* 153, 177–197.
- Bown, P.R., Rutledge, D.C., Crux, J.A., Gallagher, L.T., 1998. Lower Cretaceous. In: Bown, P.R. (Ed.), Calcareous nannofossil biostratigraphy. Chapman and Hall, Cambridge, United Kingdom, pp. 86–131.
- Bralower, T.J., Cobabe, E., Sliter, W.V., Osburn, C.L., Longoria, J., 1999. The record of global change in mid-Cretaceous (Barremian–Albian) sections from the Sierra Madre, Northeastern Mexico. *Journal of Foraminiferal Research* 29, 418–437.
- Bralower, T.J., Sliter, W.V., Arthur, M.A., Leckie, R.M., Allard, D., Schlanger, S.O., 1993. Dysoxic/anoxic episodes in the Aptian–Albian (Early Cretaceous). In: Pringle, M.S., Sager, W.W., Sliter, W.V., Stein, S. (Eds.), The Mesozoic Pacific: geology, tectonics, and volcanism: a volume in memory of Sy Schlanger, American Geophysical Union Monograph Series, 77, pp. 5–37.
- Bréhéret, J.-G., 1997. L'Aptien et l'Albien de la Fosse Voconienne (bordures et basin): Évolution de la sedimentation et enseignements sur les événements anoxiques. In: Publication Société Géologique du Nord, No. 25, 614 pp.
- Bréhéret, J.-G., Delamette, M., 1989. Faunal fluctuations related to oceanographical changes in the Vocontian basin (SE France) during Aptian-Albian time. *Geobios Memorie Speciale*, No. 11, 267–277.
- Broecker, W.S., Peng, T.H., 1982. Tracers in the Sea. Eldigio Press, Lamont Doherty Geological Observatory, Palisades, N.Y., 690 p.
- Calvert, S.E., Pedersen, T.F., 1992. Organic carbon accumulations and preservation in marine sediments: how important is anoxia? In: Whelan, J.K., Farrington, J.W. (Eds.), Productivity, accumulation and preservation of organic matter in recent and ancient sediments. Columbia University Press, New York, NY, pp. 231–263.
- Canfield, D.E., Raiswell, R., Westrich, J.T., Reaves, C.M., Berner, R.A., 1986. The use of chromium reduction in the analysis of reduced inorganic sulfur in sediments and shales. *Chemical Geology* 54, 149–155.
- Coccioni, R., Galeotti, S., 1993. Orbitally induced cycles in benthonic foraminiferal morphogroups and trophic structure distribution patterns from the Late Albian "Amadeus Segment" (Central Italy). *Journal of Micropaleontology* 12, 227–239.
- Coccioni, R., Jovane, L., Bancalà, G., Bucci, C., Fauth, G., Frontalini, F., Janikian, L., Savian, J., Paes de Almeida, R., Luz Mathias, G., van Ferreira da Trindade, R.I., April 2012. Umbria–Marche Basin, Central Italy: a Reference Section for the

- Aptian–Albian Interval at Low Latitudes. Scientific Drilling, No. 13. <http://dx.doi.org/10.2204/iodp.sd.13.07.2011>.
- Cruse, A.M., Lyons, T.W., 2004. Trace metal records of regional paleoenvironmental variability in Pennsylvanian (Upper Carboniferous) black shales. *Chemical Geology* 206, 319–345.
- Emeis, K.-C., Weissert, H., 2009. Tethyan–Mediterranean organic carbon-rich sediments from Mesozoic black shales to sapropels. *Sedimentology* 56, 247–266. <http://dx.doi.org/10.1111/j.1365-3091.200801026.x>.
- Emerson, S., Hedges, J.I., 1988. Processes controlling the organic carbon content of open ocean sediments. *Paleoceanography* 3. <http://dx.doi.org/10.1029/PA003i005p00621>.
- Erba, E., 1994. Nannofossils and superplumes: the Early Aptian “nannoconid crisis”. *Paleoceanography* 9, 483–501.
- Erbacher, J., Hemleben, C., Huber, B.T., Markey, M., 1999. Correlating environmental changes during early Albian oceanic anoxic event 1b using benthic foraminiferal paleoecology. *Marine Micropaleontology* 38, 7–28.
- Erbacher, J., Thurow, J., Little, R., 1996. Evolution patterns of radiolarian and organic matter variations: a new approach to identify sea-level changes in mid-Cretaceous pelagic environments. *Geology* 24, 499–502.
- Erbacher, J., Thurow, J., 1997. Influence of oceanic anoxic events on the evolution of mid-Cretaceous radiolaria in the North Atlantic and western Tethys. *Marine Micropaleontology* 30, 139–158.
- Föllmi, K.B., 2012. Early Cretaceous life, climate and anoxia. *Cretaceous Research* 35, 230–257.
- Foucher, J.-C., Monteil, E., 1998. Dinoflagellate cysts. In: de Graciansky, P.-C., Hardenbol, J., Jacquin, Th., Vail, P.R. (Eds.), *Mesozoic–Cenozoic sequence stratigraphy of European Basin*, SEPM (Society for Sedimentary Geology) Special Publication No. 60, pp. 770–772 (chart 5).
- Friedman, I., O’Neil, J.R., 1977. Compilation of stable isotope fractionation factors of geochemical interest. In: Fleischer, M. (Ed.), *Data of geochemistry*, U.S. Geological Survey Professional Paper 440-KK, pp. 1–12.
- Gale, A.S., Bown, P., Caron, M., Crampton, J., Crowhurst, S.J., Kennedy, W.J., Petrizzi, M.R., Wray, D.S., 2011. The uppermost Middle and Upper Albian succession at the Col de Palluel, Hautes-Alpes, France: an integrated study (ammonites, inoceramid bivalves, planktonic foraminifera, nannofossils, geochemistry, stable oxygen and carbon isotopes, cyclostratigraphy). *Cretaceous Research* 32, 59–130.
- Gale, A.S., Kennedy, W.J., Burnett, J.A., Caron, M., Kidd, B.E., 1996. The Late Albian to Early Cenomanian succession at Mont Risou near Rosans (Drome, SE France): an integrated study (ammonites, inoceramids, planktonic foraminifera, nannofossils, oxygen and carbon isotopes). *Cretaceous Research* 17, 515–606.
- Galeotti, S., Sprovieri, M., Coccioni, R., Bellanca, A., Neri, R., 2003. Orbitally modulated black shale deposition in the upper Albian Amadeus Segment (central Italy): a multi-proxy reconstruction. *Palaeogeography, Palaeoclimatology, Palaeoecology* 190, 441–458.
- Gilhooley III, W.P., Macko, S.A., Flemings, P.B., 2008. Data report: isotope compositions of sedimentary organic carbon and total nitrogen from Brazos-Trinity Basin IV (sites U1319 and U1320) and Ursa Basin (sites U1322 and U1324), deepwater Gulf of Mexico. Proceedings of the Integrated Ocean Drilling Program 308. <http://dx.doi.org/10.2204/iodp.proc.308.208.2008>.
- Gill, B.C., Lyons, T.W., Young, S.A., Kump, L.R., Knoll, A.H., Saltzman, M.R., 2011. Geochemical evidence for widespread euxinia in the Late Cambrian ocean. *Nature* 469, 80–83.
- Gromet, L.P., Dymek, R.F., Haskin, L.A., Korotev, R.L., 1984. The “North American shale composite”: its compilation, major and trace element characteristics. *Geochimica et Cosmochimica Acta* 48, 2469–2482.
- Haig, D.W., Lynch, D.A., 1993. A late early Albian marine transgressive pulse over northeastern Australia, precursor to epeiric basin anoxia: foraminiferal evidence. *Marine Micropaleontology* 22, 311–362.
- Hallam, A., 1985. Pre-Quaternary sea-level changes. *Annual Review of Earth and Planetary Sciences* 12, 205–243.
- Haq, B.U., Hardenbol, J., Vail, P.R., 1987. Chronology of fluctuating sea levels since the Triassic. *Science* 235 (4793), 1156–1167.
- Herrle, J.O., Köbler, P., Friedrich, O., Erlenkeuser, H., Hemleben, C., 2004. High-resolution carbon isotope records of the Aptian to Lower Albian from SE France and the Mazagan Plateau (DSDP Site 545): a stratigraphic tool for paleoceanographic and paleobiologic reconstruction. *Earth and Planetary Science Letters* 218, 149–161.
- Jahren, A.H., Arens, N.C., Sarmiento, G., Guerrero, J., Amundson, R., 2001. Terrestrial record of methane hydrate dissociation in the Early Cretaceous. *Geology* 29, 159–162. [http://dx.doi.org/10.1130/0091-613\(2001\)029<0159:TROMHD>2.0.CO;2](http://dx.doi.org/10.1130/0091-613(2001)029<0159:TROMHD>2.0.CO;2).
- Jarvis, I., Gale, A.S., Jenkyns, H.C., Pearce, M.A., 2006. Secular variation in Late Cretaceous carbon isotopes: a new $\delta^{13}\text{C}$ carbonate reference curve for the Cenomanian–Campanian (99.6–70.6 Ma). *Geological Magazine* 143, 561–608.
- Jenkyns, H.C., 2010. Geochemistry of oceanic anoxic events. *Geochemistry Geophysics Geosystems* 11, Q03004. <http://dx.doi.org/10.1029/2009GC002788>.
- Jenkyns, H.C., Gale, A.S., Corfield, R.M., 1994. Carbon- and oxygen-isotope stratigraphy of the English Chalk and Italian Scaglia and its palaeoclimatic significance. *Geological Magazine* 131, 1–34. <http://dx.doi.org/10.1017/S0016756800010451>.
- Jenkyns, H.C., Wilson, P.A., 1999. Stratigraphy, paleoceanography, and evolution of Cretaceous Pacific guyots: relics from a greenhouse Earth. *American Journal of Science* 299, 341–392.
- Kennedy, W.J., Cobban, W.A., Hancock, J.M., Gale, A.S., 2005. Upper Albian and Lower Cenomanian ammonites from the Main Street Limestone, Grayson Marl and Del Rio Clay in Northeast Texas. *Cretaceous Research* 26, 349–428.
- Kennedy, W.J., Gale, A.S., Hancock, J.M., Crampton, J.S., Cobban, W.A., 1999. Ammonites and inoceramid bivalves from close to the Middle–Upper Albian boundary around Fort Worth, Texas. *Journal of Paleontology* 73, 1101–1125.
- Kennedy, W.J., Gale, A.S., Lees, J.A., Caron, M., 2004. The Global Boundary Stratotype Section and Point for the base of the Cenomanian Stage, Mont Risou, Hautes-Alpes, France. *Episodes* 27, 21–32.
- Kuyper, M.M.M., Pancost, R.D., Nijenhuys, I.A., Sinnigh Damste, J.S., 2002. Enhanced productivity led to increased organic carbon burial in the euxinic North Atlantic basin during the late Cenomanian oceanic anoxic event. *Paleoceanography* 17. <http://dx.doi.org/10.1029/2000PA000569>.
- Larson, R.L., Erba, E., 1999. Onset of the Mid-Cretaceous greenhouse in the Barremian–Aptian: igneous events and the biological, sedimentary, and geochemical responses. *Paleoceanography* 14, 663–678. <http://dx.doi.org/10.1029/1999PA900040>.
- Leckie, R.M., Bralower, T.J., Cashman, R., 2002. Oceanic anoxic events and plankton evolution: biotic response to tectonic forcing during the mid-Cretaceous. *Paleoceanography* 17. <http://dx.doi.org/10.1029/2001PA000623>.
- Lovejoy, E.M.P., 1976. *Geology of Cerro de Cristo Rey uplift, Chihuahua and New Mexico*. New Mexico Bureau of Mines and Mineral Resources. Memoir 31, 84.
- Lucas, S.G., Krainer, K., Spielmann, J.A., 2010. Cretaceous stratigraphy, paleontology, petrography, depositional environments, and cycle stratigraphy at Cerro de Cristo Rey, Doña Ana County, New Mexico, New Mexico. *Geology* 32, 103–130.
- Lyons, T.W., Anbar, A.D., Severmann, S., Scott, C., Gill, B.C., 2009. Tracking euxinia in the ancient ocean: A multiproxy perspective and Proterozoic case study. *Annual Review of Earth and Planetary Sciences* 37, 507–534.
- Lyons, T.W., Severmann, S., 2006. A critical look at iron paleoredox proxies: new insights from modern euxinic marine basins. *Geochimica et Cosmochimica Acta* 70, 5698–5722.
- März, C., Poulton, S.W., Beckman, B., Küster, K., Wagner, T., Kasten, S., 2008. Redox sensitivity of P cycling during marine black shale formation: dynamics of sulfidic and anoxic, non-sulfidic bottom waters. *Geochimica et Cosmochimica Acta* 72, 3703–3717.
- Menegatti, A.P., Weissert, H., Brown, R.S., Tyson, R.V., Farrimond, P., Strasser, A., Caron, M., 1998. High-resolution $\delta^{13}\text{C}$ stratigraphy through the early Aptian “Livello Selli” of the Alpine Tethys. *Paleoceanography* 13, 530–545.
- Meyers, P.A., 1994. Preservation of elemental and isotopic source identification of sedimentary organic matter. *Chemical Geology* 114, 289–302.
- Meyers, P.A., 1997. Organic geochemical proxies of paleoceanographic, paleolimnologic, and paleoclimatic processes. *Organic Geochemistry* 27, 213–250.
- Monreal, R., Longoria, J.F., 1999. A revision of the Upper Jurassic and Lower Cretaceous stratigraphic nomenclature for the Chihuahua Trough, north-central Mexico: implications for lithocorrelations. In: Bartolini, C., Wilson, J.L., Lawton, T.F. (Eds.), *Mesozoic sedimentary and tectonic history of North-Central Mexico*. Geological Society of America, Special Publication 340, pp. 69–92.
- Morford, J.L., Emerson, S., 1999. The geochemistry of redox sensitive trace metals in sediments. *Geochimica et Cosmochimica Acta* 63, 1735–1750.
- Norland, W.D., 1986. Thermal maturation of the Mesilla Valley shale (Late Albian) on the north and east flanks of the Cerro de Cristo Rey pluton, Doña Ana County, New Mexico. The University of Texas at El Paso, El Paso, TX, 164 p. (MSc. thesis).
- Ogg, J.G., Agterberg, F.P., Gradstein, F.M., 2004. The Cretaceous Period. In: Gradstein, F., Ogg, J.G., Smith, A. (Eds.), *A Geologic time Scale*. Cambridge University Press, Cambridge, UK, pp. 344–383.
- Ogg, J.G., Hinnov, L.A., Huang, C., 2012. Cretaceous. In: Gradstein, F.M., Ogg, J.G., Schmitz, M.D., Ogg, G.M. (Eds.), *The Geologic time scale 2012*. Elsevier, Amsterdam, pp. 793–853.
- Phelps, R.M., 2011. Middle–Hauterivian to Lower–Campanian Sequence Stratigraphy and stable isotope geochemistry of the Comanche Platform, South Texas. The University of Texas, Austin, 226 p. (Unpublished Ph.D. dissertation).
- Poulton, S.W., Canfield, D.E., 2005. Development of a sequential extraction procedure for iron: implications for iron partitioning in continental derived particulates. *Chemical Geology* 214, 209–221.
- Poulton, S.W., Raiswell, R., 2002. The low-temperature geochemical cycle of iron: from continental fluxes to marine sediment deposition. *American Journal of Science* 302, 774–805.
- Pratt, L.M., King, J.D., 1986. Variable marine productivity and high eolian input recorded by rhythmic black shales in mid-Cretaceous pelagic deposits from Central Italy. *Paleoceanography* 4, 507–522.
- Price, G.D., 1999. The evidence and implications of polar ice during the Mesozoic. *Earth-Science Reviews* 48, 183–210.
- Railsback, L.B., Holland, S.M., Hunter, D.M., Jordan, E.M., Diaz, J.R., Crowe, D.E., 2003. Controls on geochemical expression of subaerial exposure in Ordovician limestones from the Nashville Dome, Tennessee, U.S.A. *Journal of Sedimentary Research* 73 (5), 790–805.
- Raiswell, R., Canfield, D.E., 1998. Sources of iron for pyrite formation in marine sediments. *American Journal of Science* 298, 219–245.
- Reboulet, S., Rawson, P.F., Moreno-Bedmar, J.A., Aguirre-Urreta, M.B., Barragán, R., Bogomolov, Y., Company, M., González-Arreola, C., Idakieva Stoyanova, V., Lukeneder, A., Matron, B., Mitta, V., Randrianaly, H., Vasicek, Z., Baraboshkin, E.J., Bert, D., Bersac, S., Bogdanova, T.N., Bulot, L.G., Latil, J.-L., Mikhailova, I.A., Ropolo, P., Szives, O., 2011. Report on the 4th International Meeting of the IUGS Lower Cretaceous Ammonite Working Group, the “Kilian Group” (Dijon, France, 30th August 2012). *Cretaceous Research* 32, 786–793.
- Rush, N.K., 2012. Upper Albian sequence stratigraphy and geochemical events in the Chihuahua Trough, South-Central New Mexico. The University of Tulsa, 98 p. (Unpublished MSc. thesis).

- Reichelt, K., 2005. Late Aptian–Albian of the Vocontian Basin (SE France) and Albian of NE-Texas: biostratigraphic and paleoceanographic implications by planktic foraminifera faunas. Eberhard-Karls-Universität Tübingen, 117 p. (Unpublished Doctoral dissertation).
- Schlanger, S.O., Jenkyns, H.C., 1976. Cretaceous oceanic anoxic events: causes and consequences. *Geologie en Mijnbouw* 55, 179–184.
- Scholle, P.A., Arthur, M.A., 1980. Carbon isotope fluctuations in Cretaceous pelagic limestones: potential stratigraphic and petroleum exploration tool. *American Association of Petroleum Geologists Bulletin* 64, 67–87.
- Scott, R.W., 2003. Introduction. In: Scott, R.W. (Ed.), *Cretaceous stratigraphy and paleoecology, Texas and Mexico*, Perkins Memorial volume, GCSSEPM Foundation, Special Publications in Geology 1, pp. vii–xiv.
- Scott, R.W., 2009. Chronostratigraphic Database for Upper Cretaceous Oceanic Red Beds (CORBs). In: Hu, X., Wang, C., Scott, R., Wagreich, M., Jansa, L. (Eds.), *Cretaceous Oceanic Redbeds: Stratigraphy, Composition, Origins, Paleogeographic, and Paleoclimatic significance*, SEPM (Society for Sedimentary Geology) Special Publication 91, pp. 31–53.
- Scott, R.W., Benson, D.G., Morin, R.W., Shaffer, B.L., Oboh-Ikuenobe, F.E., 2003. Integrated Albian–lower Cenomanian chronostratigraphy standard, Trinity River section, Texas. In: Scott, R.W. (Ed.), *Cretaceous stratigraphy and paleoecology, Texas and Mexico*, Perkins Memorial volume, GCSSEPM Foundation, Special Publications in Geology 1, pp. 277–334.
- Scott, R.W., Holbrook, J.M., Evetts, M.J., Oboh-Ikuenobe, F.E., 2001. Albian–Cenomanian depositional cycles transgressed from Chihuahua Trough to Western Interior. In: Lucas, S.G., Ulmer-Scholle, D. (Eds.), *Geology of the Llano Estacado, New Mexico Geological Society, Guidebook 52*, pp. 221–228.
- Scott, R.W., Laali, H., Fee, D.W., 1975. Density-current strata in Lower Cretaceous Washita Group, north-central Texas. *Journal of Sedimentary Petrology* 45, 562–575.
- Scott, R.W., Oboh-Ikuenobe, F.E., Benson Jr., D.G., Holbrook, J.M., 2009. Numerical age calibration of the Albian/Cenomanian boundary. *Stratigraphy* 6, 17–32.
- Scott, R.W., Schlager, W., Fouke, B., Nederbragt, S.A., 2000. Are Mid-Cretaceous eustatic events recorded in Middle East carbonate platforms? In: Alsharhan, A.S., Scott, R.W. (Eds.), *Middle East Models of Jurassic/Cretaceous Carbonate Systems*, SEPM (Society for Sedimentary Geology) Special Publication No. 69, pp. 77–88.
- Severmann, S., Lyons, T.W., Anbar, A., McManus, J., Gordon, G., 2008. Modern iron isotope perspective on the benthic iron shuttle and the redox evolution of the ancient ocean. *Geology* 36, 487–490.
- Skelton, P.W., Spicer, R.A., Kelley, S.P., Gilmour, I., 2003. *The Cretaceous world*. Cambridge University Press, Cambridge, UK, 360 p.
- Strain, W.S., 1968. Cerro de Muleros (Cerro de Cristo Rey). In: *Delaware Basin Exploration Guide, Publication 68–55*. West Texas Geological Society, p. 82.
- Strain, W.S., 1976. New formation names in the Cretaceous at Cerro de Cristo Rey, Doña Ana County, New Mexico. In: Lovejoy, E.M.P. (Ed.), *Geology of Cerro de Cristo Rey uplift, Chihuahua and New Mexico, New Mexico Bureau of Mines and Mineral Resources, Memoir 31*, pp. 77–82.
- Strasser, A., Caron, M., Gjermeni, M., 2001. The Aptian, Albian and Cenomanian of Roter Sattel, Romandes Prealps, Switzerland: a high-resolution record of oceanographic changes. *Cretaceous Research* 22, 173–199.
- Taylor, S.R., McLennan, S.M., 1985. The continental crust: its composition and evolution. Blackwell Scientific Publications, Palo Alto, CA, 328 p.
- Tejada, M.L.G., Suzuki, K., Kuroda, J., Coccioni, R., Mahoney, J.J., Ohkouchi, N., Sakamoto, T., Tatsumi, Y., 2009. Ontong Java Plateau eruption as a trigger for the early Aptian oceanic anoxic event. *Geology* 37, 855–858.
- Tribouillard, N., Algeo, T.J., Lyons, T.W., Riboulleau, A., 2006. Trace metals as paleoredox and paleoproductivity proxies: an update. *Chemical Geology* 232, 12–32.
- Voigt, S., Gale, A.S., Voigt, T., 2006. Sea-level change, carbon cycling and paleoclimate during the Late Cenomanian of northwest Europe; an integrated palaeoenvironmental analysis. *Cretaceous Research* 27, 836–858.
- Werne, J.P., Sageman, B.B., Lyons, T.W., Hollander, D.J., 2002. An integrated assessment of a “type euxinic” deposit: evidence for multiple controls on black shale deposition in the Middle Devonian Oatka creek formation. *American Journal of Science* 302, 110–143.
- Wilson, P.A., Norris, R.D., 2001. Warm tropical ocean surface and global anoxia during the mid-Cretaceous period. *Nature* 412, 425–429. <http://dx.doi.org/10.1038/35086553>.
- Young, K., 1986. Cretaceous, marine inundations of the San Marcos Platform, Texas. *Cretaceous Research* 7, 117–140.

Appendix A. Supplementary data

Supplementary data related to this article can be found online at <http://dx.doi.org/10.1016/j.cretres.2013.08.011>.